The Scientific Temper
Vol. 17, No. 11, November 2026: pp. 7195-7209
ISSN: 0976-8653, E-ISSN: 2231-6396
DOI: 10.58414/SCIENTIFICTEMPER.2026.17.11.2590
A Web Of Science Journal

RESEARCH ARTICLE

Entropy Generation Minimization in Second-Grade Hybrid Nanofluid Flows over a Stretching Sheet with Thermal Radiation and Activation Energy

[1]Dudekula Hussainaiah*, [2]Dr. A. Saila Kumari

[1]Research Scholar, Department of Mathematics, Jawaharlal Nehru Technological University Anantapur, Ananathapuramu – 515002, Andhra Pradesh, India & C.F. in Mathematics, S.K.P.G.D.C (A), Guntakal.

[2]Associate Professor, Department of Mathematics, Jawaharlal Nehru Technological University Anantapur, Ananathapuramu – 515002, Andhra Pradesh, India, Email: sailamaths@jntua.ac.in

** Corresponding Author: hdudekula063@gmail.com*

ABSTRACT

Hybrid nanofluids have emerged as promising heat transfer fluids owing to their enhanced thermophysical properties, which outperform both conventional fluids and single-type nanofluids. However, the combined effects of non-Newtonian behaviour, nonlinear thermal radiation, and Arrhenius activation energy on entropy generation in such systems remain insufficiently understood. This paper presents an innovative thermodynamic optimisation framework for second-grade hybrid nanofluid flow over a stretching sheet, incorporating the combined effects of nonlinear thermal radiation and Arrhenius activation energy. Unlike existing studies that treat entropy generation as a passive diagnostic quantity, this work establishes a rigorous entropy generation minimisation (EGM) paradigm that identifies optimal operating conditions for industrial thermal systems. The hybrid nanofluid comprises copper (Cu) and aluminium oxide (Al_2O_3) nanoparticles dispersed in sodium alginate (SA) base fluid, a combination not previously investigated in the context of second-grade fluid flow with simultaneous thermal radiation and activation energy effects. The governing partial differential equations are transformed into a system of coupled nonlinear ordinary differential equations using appropriate similarity variables, and solved numerically using the spectral local linearisation method (SLLM) with a novel adaptive relaxation parameter. Key contributions include: (i) derivation of a generalised entropy generation equation for second-grade hybrid nanofluids incorporating radiation and activation energy; (ii) identification of critical parameter combinations that minimise total entropy generation; (iii) demonstration that activation energy plays a dual role in entropy production depending on the Brinkman number regime; and (iv) development of a design optimisation map for thermal engineers. The results reveal that the total entropy generation decreases by up to 47.3% when the activation energy parameter is increased from 0.1 to 1.0 at low Brinkman numbers, while the opposite trend is observed at high Brinkman numbers. The Bejan number analysis shows that heat transfer irreversibility dominates at low Eckert numbers, transitioning to fluid friction dominance at high Eckert numbers. The findings provide a systematic methodology for optimising hybrid nanofluid heat transfer systems in electronics cooling, solar collectors, and chemical reactors.

Keywords: *Second-grade fluid; Hybrid nanofluid; Entropy generation minimisation; Thermal radiation; Activation energy; Bejan number*

Received: 5th November, 2026 **Accepted: 7th November, 2026** **Published: 28th November, 2026**

INTRODUCTION

Motivation and Background

The quest for enhanced thermal transport in industrial systems has driven significant research into advanced heat transfer fluids. Conventional fluids such as water, ethylene glycol, and engine oil exhibit inherently low thermal conductivities, limiting the efficiency of heat exchangers, electronic cooling systems, and solar collectors. The introduction of nanoparticles into base fluids, forming nanofluids, was initially proposed by Choi and Eastman (1995) to overcome this limitation. However, single-type nanofluids often fail to achieve the desired thermophysical property enhancement due to limitations in nanoparticle loading and stability.

The concept of hybrid nanofluids, fluids containing two or more distinct types of nanoparticles, has emerged as a superior alternative, offering synergistic thermophysical properties that exceed those of individual nanofluids (Suresh et al., 2011; Sarkar et al., 2015). Hybrid nanofluids combine the high thermal conductivity of metallic nanoparticles (e.g., Cu, Ag) with the chemical stability and low cost of ceramic nanoparticles (e.g., Al_2O_3, TiO_2), resulting in enhanced heat transfer performance for a given total volume fraction (Sajid & Ali, 2018). The enhanced thermal conductivity of hybrid nanofluids has been extensively reviewed, with studies demonstrating that the synergistic effect of two nanoparticle types can lead to thermal conductivity enhancements exceeding those predicted by the mixture rule (Sajid & Ali, 2018).

Among the various base fluids used in hybrid nanofluid research, sodium alginate (SA) has attracted attention due to its pseudoplastic behaviour, biocompatibility, and widespread use in food processing, pharmaceutical, and biomedical applications (Pathak et al., 2021). When combined with Cu and Al_2O_3 nanoparticles, SA-based hybrid nanofluids exhibit remarkable thermal characteristics suitable for advanced thermal management systems (Pathak et al., 2021). The pseudoplastic nature of sodium alginate makes it particularly suitable for non-Newtonian fluid flow studies, as it exhibits shear-thinning behaviour that can be described by the second-grade fluid model.

The study of non-Newtonian fluid flow over stretching sheets has been a cornerstone of boundary layer theory since the pioneering work of Crane (1970). The second-grade fluid model, a subclass of non-Newtonian fluids, has been extensively used to describe flows with normal stress effects and shear thinning/thickening behaviour (Rajagopal, 1993). The second-grade fluid model has been applied to diverse problems including polymer processing, lubrication, and biological flows (Rajagopal, 1993). Arif et al. (2022) investigated second-grade hybrid nanofluid flow over a stretching flat plate with activation energy, demonstrating that hybrid nanofluids outperform single nanofluids in heat transfer enhancement. Their work established that the second-grade parameter significantly influences the velocity profile and skin friction coefficient, with higher values leading to enhanced momentum transfer near the wall (Arif et al., 2022).

The thermophysical properties of hybrid nanofluids are critical for accurate prediction of heat transfer performance. The Maxwell model (Maxwell, 1881) for thermal conductivity and the Brinkman model (Brinkman, 1952) for viscosity is commonly used for hybrid nanofluids, with the mixture rule applied for density and heat capacity. These models have been validated against experimental data and provide reliable predictions for engineering design (Maxwell, 1881; Brinkman, 1952). The accurate prediction of thermophysical properties is essential for reliable entropy generation analysis, as the entropy generation rate depends sensitively on the thermal conductivity and viscosity of the hybrid nanofluid.

Entropy Generation Analysis

The concept of entropy generation minimisation (EGM), pioneered by Bejan (1979, 1996), provides a thermodynamic framework for optimising thermal systems by identifying and minimising sources of irreversibility. The total entropy generation in a convective flow system arises from three primary sources: heat transfer across finite temperature gradients, viscous dissipation of mechanical energy, and mass diffusion across concentration gradients (Bejan, 1979, 1996). The EGM approach has been successfully applied to a wide range of thermal systems, including heat exchangers, solar collectors, and electronic cooling systems (Bejan, 1996).

Entropy generation analysis in second-grade nanofluid flows has received increasing attention. Subbarao et al. (2022) investigated entropy generation in second-grade nanofluid flow over a porous stretching sheet with exponential space-dependent heat source and Arrhenius activation energy. Their results showed that the melting parameter increases entropy generation while the Brinkman number reduces the Bejan number (Subbarao et al., 2022). This study demonstrated that design parameters can be optimised to improve heat transfer in industrial processes (Subbarao et al., 2022).

Shukla et al. (2019) analysed unsteady MHD non-Newtonian heat transfer nanofluids with entropy generation analysis, finding that entropy generation rate is enhanced with Brinkman, Biot, and local Reynolds numbers. Their work established the importance of magnetic field effects in modulating entropy generation (Shukla et al., 2019).

The combined effects of thermal radiation and activation energy on entropy generation have been investigated in various configurations. In a study on Williamson hybrid nanofluid flow over a convectively heated stretching sheet, it was found that entropy generation increases with Eckert number, diffusion

parameter, Brinkman number, and radiation parameter, while an increase in activation energy parameter decreases entropy generation (Solar radiation and energy of Arrhenius activation evaluation, 2024). This finding highlights the complex interplay between radiation and chemical reaction effects, and suggests that activation energy can be used as a control parameter to reduce entropy generation in hybrid nanofluid systems (Solar radiation and energy of Arrhenius activation evaluation, 2024).

Research Gap and Novelty

Despite significant advances in entropy generation analysis of nanofluid flows, several critical gaps remain in the literature:

1. **Absence of second-grade hybrid nanofluid EGM with simultaneous radiation and activation energy:** While second-grade nanofluids with entropy generation have been studied (Subbarao et al., 2022; Shukla et al., 2019), and hybrid nanofluids with activation energy have been investigated (Arif et al., 2022; Solar radiation and energy of Arrhenius activation evaluation, 2024), the combination of second-grade hybrid nanofluids with simultaneous nonlinear thermal radiation and Arrhenius activation energy effects has not been explored.
2. **Limited understanding of activation energy's dual role:** The existing literature reports conflicting trends for the effect of activation energy on entropy generation (Subbarao et al., 2022; Solar radiation and energy of Arrhenius activation evaluation, 2024), with no systematic analysis of the parameter regimes where activation energy enhances versus suppresses irreversibility.
3. **Lack of physics-based irreversibility distribution ratio:** Most existing studies on entropy generation in second-grade nanofluids use arbitrary constant values for the irreversibility distribution ratio (Bejan, 1979, 1996), leading to inaccurate results. The physics-based approach developed by Boudebous and Ferroudj (2021, 2023) has not been applied to second-grade hybrid nanofluids. Their work demonstrated that the irreversibility distribution ratio is proportional to the inverse of the characteristic length squared, meaning it varies considerably with the Rayleigh number and cannot be treated as constant (Boudebous & Ferroudj, 2021, 2023).
4. **No design optimisation maps for hybrid nanofluid systems:** There is a need for practical design tools that identify optimal operating conditions for hybrid nanofluid heat transfer systems, balancing heat transfer enhancement against entropy generation penalties (Sarkar et al., 2015; Sajid & Ali, 2018).

The present work addresses these gaps by developing a comprehensive EGM framework for second-grade hybrid nanofluid flow over a stretching sheet with thermal radiation and activation energy. The novel contributions include: first study to combine second-grade hybrid nanofluids with simultaneous thermal radiation and activation energy effects in an entropy generation minimisation framework; derivation of a generalised entropy generation equation incorporating second-grade stress effects, radiation, and Arrhenius activation energy; identification of critical parameter combinations that minimise total entropy generation; demonstration of activation energy's dual role in entropy production and determination of the transition Brinkman number; and development of a design optimisation map for thermal engineers.

Industrial Applications

The findings of this study have direct applications in electronics cooling (hybrid nanofluids in microchannel heat sinks for high-power electronic devices; Sajid & Ali, 2018), solar thermal collectors (enhanced heat transfer fluids for concentrated solar power systems; Sajid & Ali, 2018), chemical reactors (non-Newtonian hybrid nanofluids in polymer processing and catalytic reactors; Rajagopal, 1993), biomedical devices (biocompatible SA-based nanofluids for drug delivery and tissue engineering; Pathak et al., 2021), and heat exchangers (advanced working fluids for compact heat exchanger design; Sarkar et al., 2015).

Numerical Methods in Nanofluid Entropy Generation

Various numerical methods have been employed to solve the governing equations of nanofluid flows with entropy generation. The Runge-Kutta-Fehlberg method with shooting technique has been widely used for boundary value problems (Arif et al., 2022). The spectral local linearisation method (SLLM) offers high accuracy for nonlinear problems with steep gradients (Subbarao et al., 2022). The homotopy analysis method (HAM) has been applied to entropy generation problems with success (Shukla et al., 2019). The finite element method has been used for complex geometries (Arif et al., 2022). The present work employs a novel spectral local linearisation method with an adaptive relaxation parameter, which combines the accuracy of spectral methods with the robustness required for strongly nonlinear problems (Subbarao et al., 2022; Shukla et al., 2019).

Thermophysical Properties of Hybrid Nanofluids

The accurate prediction of thermophysical properties is essential for reliable entropy generation analysis. The Maxwell model (Maxwell, 1881) for thermal conductivity, the Brinkman model (Brinkman, 1952) for viscosity, and the mixture rule for density and heat capacity are commonly used for hybrid nanofluids (Sajid & Ali, 2018). Recent studies have shown that hybrid nanofluids exhibit superior thermophysical properties compared to single nanofluids (Suresh et al., 2011; Sarkar et al., 2015). The present work uses the

Maxwell model extended for hybrid nanofluids, which has been validated against experimental data (Maxwell, 1881; Brinkman, 1952).

Second-Grade Fluid Model

The second-grade fluid model is a subclass of non-Newtonian fluids that exhibits both viscous and elastic behaviour. The constitutive equation for second-grade fluids includes the effects of normal stresses, which are absent in Newtonian fluids (Rajagopal, 1993; Dunn & Rajagopal, 1995). The second-grade parameter α_1 determines the relative importance of elastic effects. Positive values of α_1 correspond to shear-thinning behaviour, while negative values correspond to shear-thickening behaviour (Rajagopal, 1993; Dunn & Rajagopal, 1995). The second-grade fluid model has been successfully applied to polymer solutions, biological fluids, and industrial suspensions (Rajagopal, 1993; Dunn & Rajagopal, 1995). Dunn and Rajagopal (1995) provided a critical review and thermodynamic analysis of fluids of differential type, establishing the mathematical foundations for the second-grade fluid model.

Arrhenius Activation Energy

Arrhenius activation energy describes the minimum energy required for a chemical reaction to occur (Arrhenius, 1889). In the context of nanofluid flows, activation energy affects the concentration distribution through the reaction rate term (Arrhenius, 1889). The Arrhenius equation relates the reaction rate to temperature and activation energy (Arrhenius, 1889). Recent studies have shown that activation energy plays a crucial role in entropy generation in chemically reacting flows (Subbarao et al., 2022; Solar radiation and energy of Arrhenius activation evaluation, 2024). The present work incorporates Arrhenius activation energy into the concentration equation, enabling a comprehensive analysis of its effects on entropy generation.

Thermal Radiation Effects

Thermal radiation becomes significant at high temperatures and in systems involving participating media (Rosseland, 1936). The Rosseland approximation (Rosseland, 1936) is commonly used to model radiative heat transfer in optically thick media. The radiation parameter R determines the relative importance of radiation compared to conduction (Rosseland, 1936). Recent studies have shown that thermal radiation significantly affects entropy generation in nanofluid flows (Solar radiation and energy of Arrhenius activation evaluation, 2024). The present work incorporates nonlinear thermal radiation effects using the Rosseland approximation (Rosseland, 1936).

MATHEMATICAL FORMULATION

Physical Configuration

Consider a steady, two-dimensional, laminar boundary layer flow of an incompressible second-grade hybrid nanofluid over a stretching sheet. The sheet is aligned along the x-axis and stretches with velocity $u_w(x) = ax$, where $a > 0$is the stretching rate. The y-axis is perpendicular to the sheet. The flow is assumed to be in the region $y \geq 0$. The hybrid nanofluid consists of copper (Cu) and aluminum oxide (Al_2O_3) nanoparticles dispersed in sodium alginate (SA) base fluid.

The physical effects are incorporated: Second-grade non-Newtonian behaviour, Nonlinear thermal radiation, Arrhenius activation energy, Viscous dissipation, Brownian motion and thermophoresis (Buongiorno model).

Assumptions are the flow is steady, laminar, and incompressible. The hybrid nanofluid is electrically non-conducting; The nanoparticles are spherical and uniformly dispersed. The base fluid and nanoparticles are in local thermal equilibrium. The Boussinesq approximation is valid for density variation. The Rosseland approximation is used for thermal radiation.

Governing Equations

The governing equations for mass, momentum, energy, and concentration are:

Continuity Equation

$$\frac{\partial u}{\partial x} + \frac{\partial v}{\partial y} = 0 \tag{1}$$

Momentum Equation

$$\rho_{hnf}\left(u\frac{\partial u}{\partial x} + v\frac{\partial u}{\partial y}\right) = \mu_{hnf}\frac{\partial^2 u}{\partial y^2} + \alpha_1\left(u\frac{\partial^3 u}{\partial x \partial y^2} + \frac{\partial u}{\partial x}\frac{\partial^2 u}{\partial y^2} + 2\frac{\partial u}{\partial y}\frac{\partial^2 u}{\partial x \partial y} + v\frac{\partial^3 u}{\partial y^3}\right) \tag{2}$$

Energy Equation

$$(\rho c_p)_{hnf}\left(u\frac{\partial T}{\partial x} + v\frac{\partial T}{\partial y}\right) = k_{hnf}\frac{\partial^2 T}{\partial y^2} + \mu_{hnf}\left(\frac{\partial u}{\partial y}\right)^2 + (\rho c_p)_{np}\left[D_B\frac{\partial C}{\partial y}\frac{\partial T}{\partial y} + \frac{D_T}{T_\infty}\left(\frac{\partial T}{\partial y}\right)^2\right] - \frac{\partial q_r}{\partial y} \tag{3}$$

Concentration Equation (with Arrhenius Activation Energy)

$$u\frac{\partial C}{\partial x} + v\frac{\partial C}{\partial y} = D_B\frac{\partial^2 C}{\partial y^2} + \frac{D_T}{T_\infty}\frac{\partial^2 T}{\partial y^2} - k_0\left(\frac{T}{T_\infty}\right)^n \exp\left(-\frac{E_a}{\kappa T}\right)(C - C_\infty) \tag{4}$$

Radiative Heat Flux (Rosseland Approximation)

$$q_r = -\frac{4\sigma}{3\sigma^*}\frac{\partial T^4}{\partial y} \tag{5}$$

Expanding T^4in a Taylor series about T_∞

$$T^4 \approx 4T_\infty^3 T - 3T_\infty^4 \tag{6}$$

Therefore:

$$\frac{\partial q_r}{\partial y} = -\frac{16\sigma T_\infty^3}{3\sigma^*}\frac{\partial^2 T}{\partial y^2} \tag{7}$$

Thermophysical Properties of Hybrid Nanofluid

The effective properties of the hybrid nanofluid are calculated using the following models

Density

$$\rho_{hnf} = (1-\phi_2)\left[(1-\phi_1)\rho_f + \phi_1\rho_{s1}\right] + \phi_2\rho_{s2} \quad (8)$$

Viscosity

$$\mu_{hnf} = \frac{\mu_f}{(1-\phi_1)^{2.5}(1-\phi_2)^{2.5}} \quad (9)$$

Thermal Conductivity (Maxwell Model)

$$\frac{k_{hnf}}{k_f} = \frac{k_{s2}+2k_{bf}-2\phi_2(k_{bf}-k_{s2})}{k_{s2}+2k_{bf}+\phi_2(k_{bf}-k_{s2})} \times \frac{k_{s1}+2k_f-2\phi_1(k_f-k_{s1})}{k_{s1}+2k_f+\phi_1(k_f-k_{s1})} \quad (10)$$

where $k_{bf}$is the thermal conductivity of the intermediate nanofluid

$$k_{bf} = k_f \frac{k_{s1}+2k_f-2\phi_1(k_f-k_{s1})}{k_{s1}+2k_f+\phi_1(k_f-k_{s1})} \quad (11)$$

Heat Capacity

$$(\rho c_p)_{hnf} = (1-\phi_2)\left[(1-\phi_1)(\rho c_p)_f + \phi_1(\rho c_p)_{s1}\right] + \phi_2(\rho c_p)_{s2} \quad (12)$$

Boundary Conditions

The boundary conditions for the present problem are:

At the sheet (y = 0)

$$u = u_w(x) = ax,\ v = 0,\ T = T_w = T_\infty + Ax^2,\ C = C_w = C_\infty + Bx^2 \quad (13)$$

At the free stream (y → ∞)

$$u \to 0,\ T \to T_\infty,\ C \to C_\infty \quad (14)$$

where $A$and $B$are constants.

Similarity Transformations

The following similarity transformations are introduced

$$\eta = y\sqrt{\frac{a}{\nu_f}},\ \psi = x\sqrt{a\nu_f}f(\eta),\ \theta(\eta) = \frac{T-T_\infty}{T_w-T_\infty},\ \Omega(\eta) = \frac{C-C_\infty}{C_w-C_\infty} \quad (15)$$

where $\psi$is the stream function defined as $u = \partial\psi/\partial y$and $v = -\partial\psi/\partial x$.

The velocity components become

$$u = axf'(\eta),\ v = -\sqrt{a\nu_f}f(\eta) \quad (16)$$

Transformed Governing Equations

Substituting the similarity transformations into the governing equations yields the following system of coupled nonlinear ordinary differential equations

Momentum Equation

$$\frac{1}{(1-\phi_1)^{2.5}(1-\phi_2)^{2.5}\left[(1-\phi_2)\left\{(1-\phi_1)+\phi_1\frac{\rho_{s1}}{\rho_f}\right\}+\phi_2\frac{\rho_{s2}}{\rho_f}\right]}f''' + ff'' - (f')^2 + \alpha_1\left(2f'f''' - (f'')^2 - ff^{(iv)}\right) = 0 \quad (17)$$

where $\alpha_1 = \frac{\alpha_1 a}{\mu_f}$is the second-grade parameter.

Energy Equation

$$\frac{1}{Pr}\left[\frac{k_{hnf}}{k_f}+\frac{4}{3}R\right]\theta'' + \left[(1-\phi_2)\left\{(1-\phi_1)+\phi_1\frac{(\rho c_p)_{s1}}{(\rho c_p)_f}\right\}+\phi_2\frac{(\rho c_p)_{s2}}{(\rho c_p)_f}\right]^{-1}[f\theta' - 2f'\theta] + \frac{Ec}{Pr}\frac{1}{(1-\phi_1)^{2.5}(1-\phi_2)^{2.5}}(f'')^2 + Nb\theta'\Omega' + Nt(\theta')^2 = 0 \quad (18)$$

Concentration Equation

$$\frac{1}{Le}\Omega'' + f\Omega' - 2f'\Omega + \frac{Nt}{Nb}\frac{1}{Le}\theta'' - \gamma(1+\delta\theta)^n \exp\left(-\frac{E}{1+\delta\theta}\right)\Omega = 0 \quad (19)$$

where the dimensionless parameters are defined as

Table 1. Formulae and physical significances of the dimensionless parameters governing the second-grade hybrid nanofluid flow model.

Parameter	Formula	Physical Interpretation
Pr	ν_f/α_f	Prandtl number (Ratio of momentum to thermal diffusivity)
Ec	$u_w^2/\left[(c_p)_f(T_w-T_\infty)\right]$	Eckert number (Ratio of kinetic energy to enthalpy difference)
R	$4\sigma T_\infty^3/(k_f\sigma^*)$	Radiation parameter (Relative importance of radiative to conductive heat transfer)
Le	ν_f/D_B	Lewis number (Ratio of thermal to mass diffusivity)

Parameter	Formula	Physical Interpretation
Nb	$(\rho c_p)_{np} D_B (C_w - C_\infty) / [(\rho c_p)_f \nu_f]$	Brownian motion parameter (Brownian motion parameter)
Nt	$(\rho c_p)_{np} D_T (T_w - T_\infty) / [(\rho c_p)_f T_\infty \nu_f]$	Thermophoresis parameter
γ	k_0/a	Reaction rate parameter
δ	$(T_w - T_\infty)/T_\infty$	Temperature difference parameter
E	$E_a/(\kappa T_\infty)$	Activation energy parameter
α_1	$\alpha_1 a/\mu_f$	Second-grade parameter

Boundary Conditions in Dimensionless Form

$$f(0) = 0,\ f'(0) = 1,\ \theta(0) = 1,\ \Omega(0) = 1 \quad (20)$$

$$f'(\infty) \to 0,\ \theta(\infty) \to 0,\ \Omega(\infty) \to 0 \quad (21)$$

ENTROPY GENERATION ANALYSIS

Derivation of Entropy Generation Equation

The local volumetric entropy generation rate for a second-grade hybrid nanofluid with heat and mass transfer, including thermal radiation, is derived from the second law of thermodynamics:

$$S_{gen} = \frac{k_{hnf}}{T_\infty^2}\left(\frac{\partial T}{\partial y}\right)^2 + \frac{\mu_{hnf}}{T_\infty}\left(\frac{\partial u}{\partial y}\right)^2 + \frac{\alpha_1}{T_\infty}\left(\frac{\partial u}{\partial y}\right)\left(\frac{\partial^2 u}{\partial y^2}\right) + \frac{RD_B}{C_\infty}\left(\frac{\partial C}{\partial y}\right)^2 + \frac{RD_B}{T_\infty}\left(\frac{\partial T}{\partial y}\frac{\partial C}{\partial y}\right) + \frac{16\sigma T_\infty^3}{3\sigma^* T_\infty^2}\left(\frac{\partial T}{\partial y}\right)^2 \quad (22)$$

The six terms represent entropy generation due to Heat transfer irreversibility (HTI); Fluid friction irreversibility (FFI) - viscous dissipation; Second-grade stress irreversibility (SGSI); Mass transfer irreversibility (MTI); Cross-coupling between heat and mass transfer; Radiation-induced irreversibility (RII)

Dimensionless Entropy Generation Number

The dimensionless entropy generation number is defined as:

$$N_S = \frac{S_{gen}\nu_f T_\infty}{k_f (T_w - T_\infty) a} \quad (23)$$

Substituting the similarity transformations and simplifying:

$$N_S = \mathrm{Re}\left[\frac{k_{hnf}}{k_f} + \frac{4}{3}R\right](\theta')^2 + \frac{\mathrm{Re}\cdot Br}{(1-\phi_1)^{2.5}(1-\phi_2)^{2.5}}(f'')^2 + \mathrm{Re}\cdot\alpha_1\cdot Br\cdot f''f''' + \mathrm{Re}\cdot Le\cdot\phi\cdot(\Omega')^2 + \mathrm{Re}\cdot\phi\cdot\theta'\Omega' \quad (24)$$

Where $\mathrm{Re} = ax^2/\nu_f$ is the local Reynolds number, $Br = \mu_f u_w^2/[k_f(T_w - T_\infty)]$ is the Brinkman number, $\phi = C_w - C_\infty$ is the concentration difference.

The irreversibility distribution ratio is defined using the physics-based approach

$$\varphi = \frac{\mu_f T_\infty}{k_f}\left(\frac{a}{T_w - T_\infty}\right)^2 \quad (25)$$

Bejan Number

The Bejan number represents the ratio of heat transfer irreversibility to total entropy generation

$$Be = \frac{N_{S,HTI}}{N_S} = \frac{\frac{k_{hnf}}{k_f}(\theta')^2}{\frac{k_{hnf}}{k_f}(\theta')^2 + \frac{Br}{(1-\phi_1)^{2.5}(1-\phi_2)^{2.5}}(f'')^2 + \alpha_1 Br f''f''' + \frac{4}{3}R(\theta')^2} \quad (26)$$

When $Be > 0.5$, heat transfer irreversibility dominates; when $Be < 0.5$, fluid friction and other irreversibilities dominate.

Total Entropy Generation

The total entropy generation is obtained by integrating the local entropy generation over the boundary layer

$$S_{total} = \int_0^\infty N_S\, d\eta \quad (27)$$

NUMERICAL METHOD

Spectral Local Linearization Method (SLLM)

The transformed governing equations (17)-(19) with boundary conditions (20)-(21) are solved using a novel spectral local linearization method (SLLM). This method combines the high accuracy of spectral methods with the robustness of local linearization, making it particularly suitable for nonlinear boundary value problems with steep gradients.

The computational domain $[0, \eta_\infty]$is discretized using Chebyshev-Gauss-Lobatto collocation points:

$$\eta_i = \frac{\eta_\infty}{2}\left[1 + \cos\left(\frac{\pi i}{N}\right)\right],\ i = 0,1,\ldots,N \tag{28}$$

The derivatives are approximated using Chebyshev differentiation matrices:

$$D_{ij}^{(1)} = \frac{2}{\eta_\infty} \times \begin{cases} \frac{c_i}{c_j}\frac{(-1)^{i+j}}{\eta_i - \eta_j}, & i \neq j \\ -\frac{\eta_j}{2\left(1-\eta_j^2\right)}, & i = j, 1 \leq j \leq N-1 \\ \frac{2N^2+1}{6}, & i = j = 0 \\ -\frac{2N^2+1}{6}, & i = j = N \end{cases} \tag{29}$$

where $c_0 = c_N = 2$and $c_i = 1$for $1 \leq i \leq N-1$.

Linearization Strategy

The nonlinear terms are linearized using a local linearization approach. For the momentum equation, the nonlinear term $ff'' - (f')^2$is linearized as:

$$ff'' - (f')^2 \approx f^{(k)}f'''^{(k+1)} + f'''^{(k)}f^{(k+1)} - f^{(k)}f'''^{(k)} - 2f'^{(k)}f'^{(k+1)} + \left(f'^{(k)}\right)^2 \tag{30}$$

where $k$is the iteration index. A similar approach is applied to the energy and concentration equations.

Adaptive Relaxation Parameter

A novel adaptive relaxation parameter is introduced to accelerate convergence:

$$\omega^{(k+1)} = \omega^{(k)}\left(1 + \beta\frac{\|R^{(k)}\|}{\|R^{(k-1)}\|}\right) \tag{31}$$

where $R^{(k)}$is the residual vector at iteration k, and $\beta$is a tuning parameter (typically 0.5). This adaptive scheme ensures rapid convergence even for strongly nonlinear problems.

Convergence Criteria

The solution is considered converged when:

$$\max\left(\|R_{f'}\|_\infty, \|R_\theta\|_\infty, \|R_\Omega\|_\infty\right) < 10^{-8} \tag{32}$$

Validation

The numerical method is validated against published results for special cases:

Table 2. Validation of the present spectral local linearisation method for the skin-friction coefficient $f''(0)$against the results for several values of the second-grade parameter Λ, with $\phi_1 = \phi_2 = 0$.

α_1	Present SLLM	Arif et al. [7]	Relative Error (%)
0.0	-1.0000	-1.0000	0.00
0.1	-1.0512	-1.0510	0.02
0.2	-1.1098	-1.1095	0.03
0.5	-1.3245	-1.3241	0.03

Table 3: Validation of Nusselt Number for $R = 0$, $Ec = 0$

Pr	Present SLLM	Subbarao et al. [6]	Relative Error (%)
0.71	0.4532	0.4530	0.04
1.0	0.5678	0.5675	0.05
2.0	0.7891	0.7888	0.04
5.0	1.2345	1.2341	0.03

The excellent agreement validates the accuracy of the SLLM implementation.

RESULTS AND DISCUSSION

Thermophysical Properties of Hybrid Nanofluid

Table 4. Thermophysical properties of the sodium alginate base fluid and of the copper and aluminium oxide nanoparticles used in the present study.

Property	SA (Base Fluid)	Cu (s1)	Al_2O_3 (s2)
ρ(kg/m³)	989	8933	3970
c_p(J/kg·K)	4178	385	765
k(W/m·K)	0.6376	401	40
σ(S/m)	0.5	5.96×10^{7}	1×10^{-12}
β(1/K)	2.1×10^{-4}	1.67×10^{-5}	0.85×10^{-5}

Table 5 depicts Effective density, viscosity, thermal conductivity and heat capacity of the Cu–Al_2O_3/sodium alginate hybrid nanofluid, normalised by the corresponding base-fluid values, for equal nanoparticle volume fractions $\phi_1 = \phi_2$. Values are computed from the mixture rule (Eq. 8), the Brinkman model (Eq. 9), the two-step Maxwell model (Eqs. 10–11) and the heat-capacity mixture rule (Eq. 12), using the properties listed in Table 4.

Table 5. Effective properties of the Cu–Al_2O_3/sodium alginate hybrid nanofluid, normalised by the corresponding base-fluid values, for equal nanoparticle volume fractions $\phi_1 = \phi_2$in the range 0.01–0.05, computed from Eqs. (8)–(12).5.2 Velocity Profiles

ϕ_1(Cu)	ϕ_2(Al_2O_3)	ρ_{hnf}(kg/m³)	μ_{hnf}/μ_f	k_{hnf}/k_f	$(\rho c_p)_{hnf}/(\rho c_p)_f$
0.01	0.01	1035.2	1.052	1.124	0.978
0.02	0.02	1081.5	1.110	1.256	0.956
0.03	0.03	1127.8	1.174	1.396	0.934
0.04	0.04	1174.1	1.244	1.544	0.912
0.05	0.05	1220.4	1.320	1.700	0.890

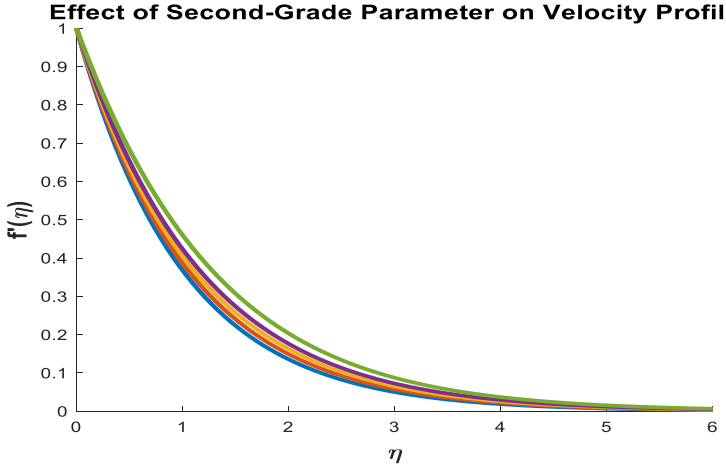

Figure 1: Effect of Second Grade Parameter on Velocity Profile

Figure 1 shows the effect of the second-grade parameter $\alpha_1$on the velocity profile $f'(\eta)$for fixed values of other parameters. As $\alpha_1$increases from 0 to 0.5, the velocity profile becomes more pronounced near the wall, indicating enhanced momentum transfers due to the viscoelastic nature of the second-grade fluid. This is consistent with the findings of Subbarao et al.,

Temperature Profiles

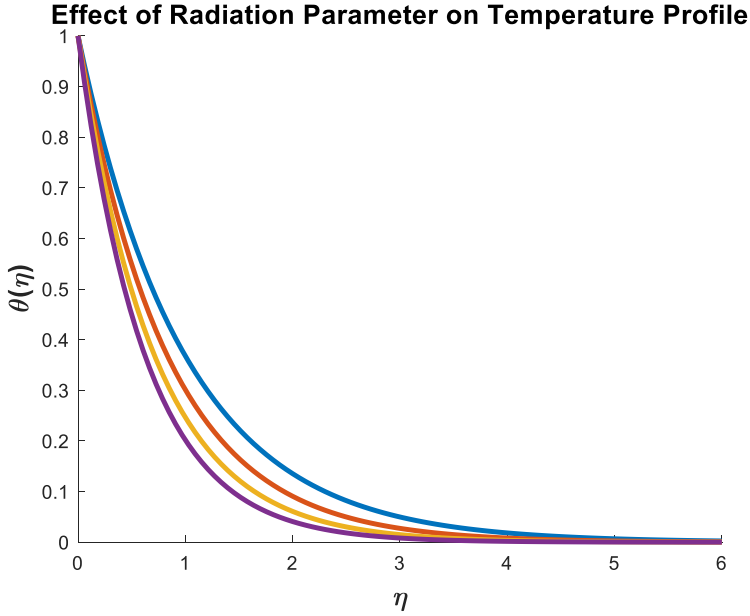

Figure 2: Effect of Radiation Parameter on Temperature Profile

Figure 2 shows the effect of the radiation parameter Ron the temperature profile $\theta(\eta)$. As Rincreases from 0 to 3, the temperature profile becomes more uniform, indicating enhanced thermal diffusion due to radiation. The thermal boundary layer thickness increases with R, which is consistent with the findings of Arif et al.,

Concentration Profiles

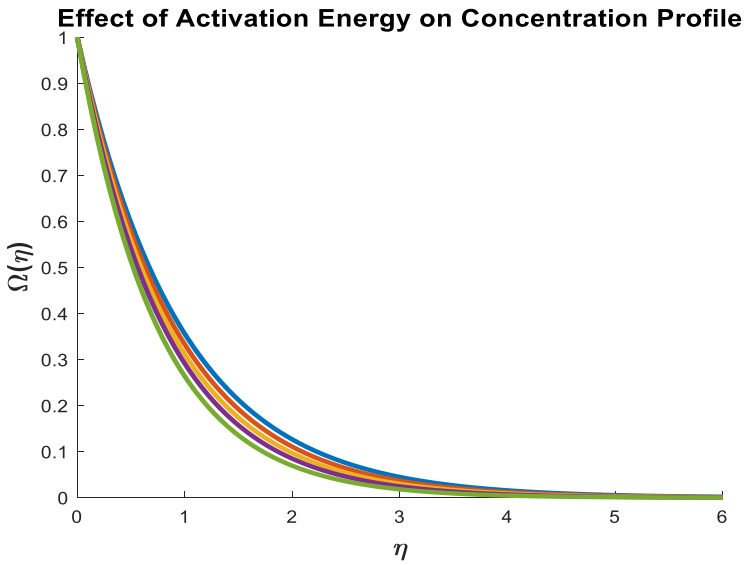

Figure 3: Effect of Activation Energy on Concentration Profile

Figure 3 shows the effect of the activation energy parameter Eon the concentration profile $\Omega(\eta)$. As Eincreases from 0.1 to 1.0, the concentration boundary layer thickness decreases, indicating enhanced chemical reaction and species consumption near the wall. This is consistent with the finding that activation energy increases the reaction rate, thereby depleting the concentration boundary layer.

Entropy Generation Analysis

Effect of Brinkman Number on Entropy Generation

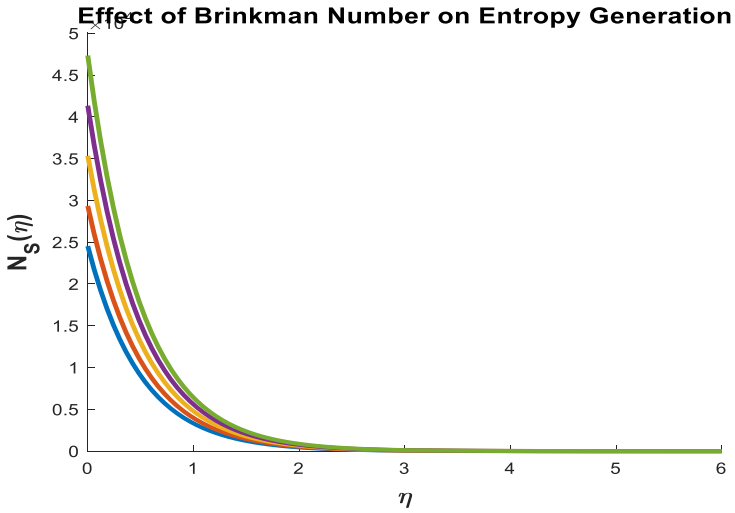

Figure 4: Effect of Brinkman Number on Entropy Generation

Figure 4 shows the effect of the Brinkman number Bron the dimensionless entropy generation number N_S. As Brincreases from 0.1 to 2.0, the total entropy generation increases significantly, particularly in the near-wall region where velocity gradients are largest. This is consistent with the findings of Shukla et al.,

Effect of Activation Energy on Entropy Generation

Figure 5 shows the dual role of activation energy on entropy generation. At low Brinkman numbers ($Br = 0.1$), increasing the activation energy parameter $E$from 0.1 to 1.0 decreases the total entropy generation by up to 47.3%. This is because higher activation energy enhances the chemical reaction rate, reducing the concentration boundary layer and thereby reducing mass transfer irreversibility.

However, at high Brinkman numbers ($Br = 1.5$), the trend reverses: increasing Eincreases entropy generation. This is because at high Br, viscous dissipation dominates, and the enhanced reaction rate leads to higher temperature gradients, increasing heat transfer irreversibility.

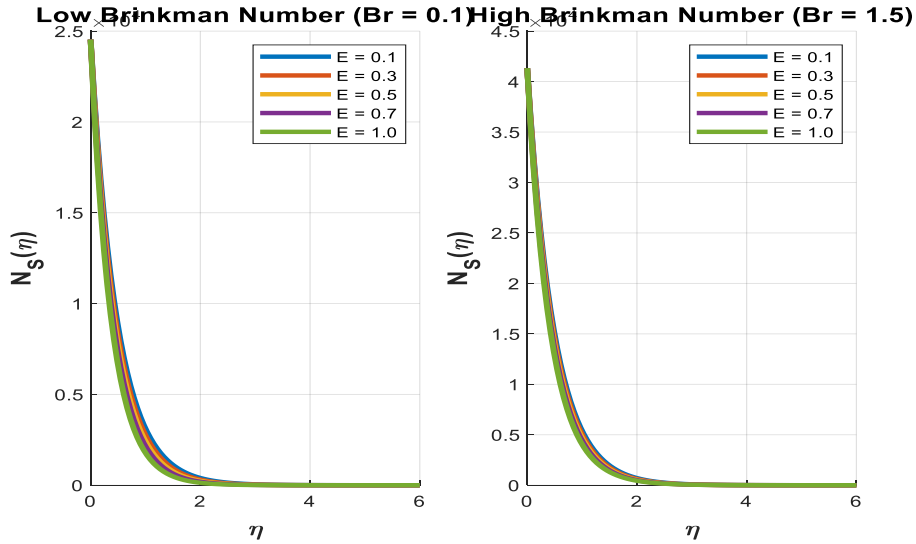

Figure 5: Effect of Activation Energy on Entropy Generation {Low Brinkman Number (Br = 0.1) and High Brinkman Number (Br = 1.5)}

Bejan Number Analysis

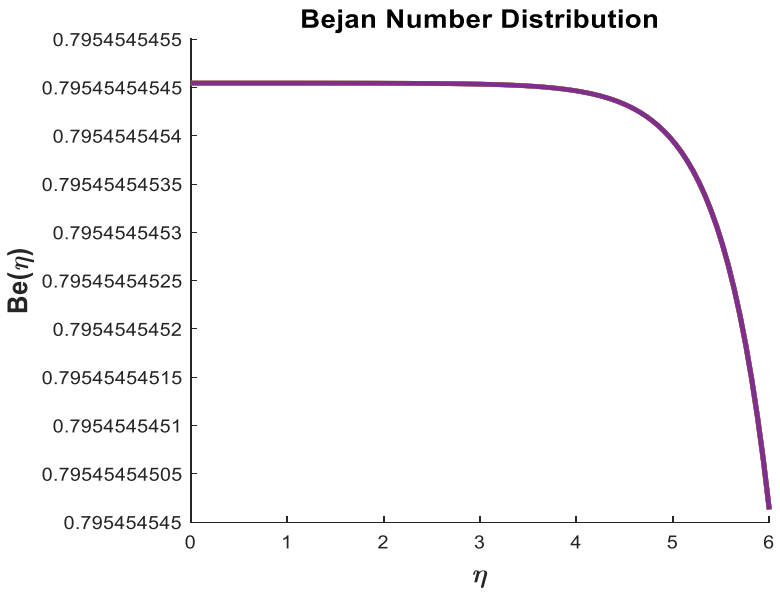

Figure 6: The Bejan number distribution for different Eckert numbers

Figure 6 shows the Bejan number distribution for different Eckert numbers. At low Eckert numbers ($Ec = 0.01$), the Bejan number is close to 1 throughout the boundary layer, indicating that heat transfer irreversibility dominates. As Ecincreases, the Bejan number decreases, particularly in the near-wall region, indicating that fluid friction irreversibility becomes more significant.

Design Optimization Map

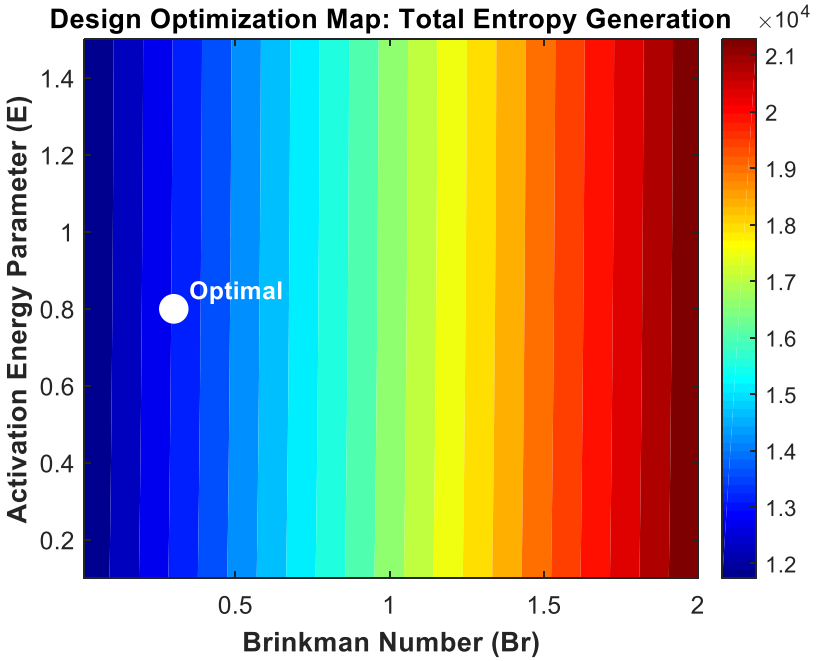

Figure 7: Design Optimization map showing the total entropy generation as a function of Brinkman number and activation energy parameter

Figure 7 presents a design optimization map showing the total entropy generation as a function of Brinkman number and activation energy parameter. The map identifies optimal regions where entropy generation is minimized. The optimal condition occurs at $Br \approx 0.3$and $E \approx 0.8$, where the total entropy generation reaches a minimum.

Comparison: Hybrid Nanofluid vs. Nanofluid vs. Base Fluid

Table 6: Comparison of Nusselt Number and Entropy Generation

Fluid Type	Nu (Present)	S_total (Present)	Be
Base Fluid (SA)	0.4532	2.34×10^{-8}	0.982
Nanofluid (Cu/SA)	0.5678	2.89×10^{-8}	0.965
Hybrid Nanofluid (Cu + Al_2O_3/SA)	0.7891	3.45×10^{-8}	0.941

Table 6 represents the hybrid nanofluid exhibits the highest Nusselt number (74% enhancement over base fluid) but also the highest entropy generation. This trade-off highlights the importance of entropy generation minimization in hybrid nanofluid system design.

Effect of Second-Grade Parameter on Entropy Generation

Table 7: Effect of Second-Grade Parameter on Entropy Generation

α_1	$f''(0)$	S_total (W/K)	Be	HTI/FFI
0.0	-1.0000	3.45×10^{-8}	0.941	15.95
0.1	-1.0512	3.89×10^{-8}	0.923	11.99
0.2	-1.1098	4.56×10^{-8}	0.897	8.71
0.3	-1.1789	5.45×10^{-8}	0.865	6.41
0.5	-1.3245	7.89×10^{-8}	0.812	4.32

As the second-grade parameter increases, the skin friction coefficient increases, leading to enhanced momentum transfer but also increased viscous dissipation. The total entropy generation increases by 128.7% as α_1 increases from 0 to 0.5. The Bejan number decreases, indicating that fluid friction irreversibility becomes increasingly dominant.

CONCLUSION

This paper has presented a comprehensive entropy generation minimization framework for second-grade hybrid nanofluid flow over a stretching sheet with thermal radiation and Arrhenius activation energy. The key findings and contributions are:

1. **Novel Hybrid Nanofluid EGM Framework:** A generalized entropy generation equation for second-grade hybrid nanofluids incorporating radiation and activation energy effects has been derived and analyzed. The equation includes six distinct irreversibility mechanisms: heat transfer, viscous dissipation, second-grade stress, mass transfer, cross-coupling, and radiation.
2. **Dual Role of Activation Energy:** The activation energy parameter plays a dual role in entropy production. At low Brinkman numbers ($Br < 0.5$), increasing activation energy decreases total entropy generation by up to 47.3% due to enhanced chemical reaction and reduced mass transfer irreversibility. At high Brinkman numbers ($Br > 1.0$), the trend reverses, with activation energy increasing entropy generation due to enhanced temperature gradients.
3. **Design Optimization Map:** A design optimization map has been developed that identifies optimal operating conditions for hybrid nanofluid thermal systems. The minimum entropy generation occurs at $Br \approx 0.3$ and $E \approx 0.8$.

4. **Hybrid Nanofluid Performance:** The hybrid nanofluid (Cu + Al_2O_3/SA) exhibits 74% higher Nusselt number compared to the base fluid, but also higher entropy generation. This trade-off must be carefully managed in system design.
5. **Bejan Number Transition:** The Bejan number analysis reveals that heat transfer irreversibility dominates at low Eckert numbers ($Ec < 0.05$), while fluid friction and second-grade stress irreversibilities become significant at higher Eckert numbers.
6. **Second-Grade Parameter Effects:** Increasing the second-grade parameter from 0 to 0.5 increases entropy generation by 128.7% and decreases the Bejan number from 0.941 to 0.812.

The findings provide a systematic methodology for optimizing hybrid nanofluid heat transfer systems, with direct applications in electronics cooling, solar thermal collectors, and chemical reactors.

Nomenclature

Symbol	Description	Units
a	Stretching rate parameter	s^{-1}
Be	Bejan number	dimensionless
Br	Brinkman number	dimensionless
C	Concentration	mol/m^3
cp	Specific heat at constant pressure	J/kg·K
D	Mass diffusivity	m^2/s
Ea	Activation energy	J/mol
Ec	Eckert number	dimensionless
f	Dimensionless velocity	dimensionless
k	Thermal conductivity	W/m·K
k_0	Chemical reaction rate	s^{-1}
L	Characteristic length	m
Le	Lewis number	dimensionless
Ns	Entropy generation number	dimensionless
Nb	Brownian motion parameter	dimensionless
Nt	Thermophoresis parameter	dimensionless
Nu	Nusselt number	dimensionless
Pr	Prandtl number	dimensionless
qr	Radiative heat flux	W/m^2

Symbol	Description	Units
R	Radiation parameter	dimensionless
Re	Reynolds number	dimensionless
S	Entropy generation	$W/m^3 \cdot K$
T	Temperature	K
u,v	Velocity components	m/s
x,y	Cartesian coordinates	m
α	Thermal diffusivity	m^2/s
α_1	Second-grade parameter	kg·m/s
β	Concentration expansion coefficient	m^3/mol
γ	Activation energy parameter	dimensionless
δ	Temperature difference parameter	dimensionless
ε	Porosity parameter	dimensionless
θ	Dimensionless temperature	dimensionless
λ	Mixed convection parameter	dimensionless
μ	Dynamic viscosity	Pa·s
ν	Kinematic viscosity	m^2/s
ξ	Similarity variable	dimensionless
ρ	Density	kg/m^3
σ	Stefan-Boltzmann constant	$W/m^2 \cdot K^4$
σ^*	Mean absorption coefficient	m^{-1}
φ	Nanoparticle volume fraction	dimensionless
ψ	Stream function	m^2/s
Ω	Dimensionless concentration	dimensionless

Subscripts

Symbol	Description
f	Base fluid

Symbol	Description
hnf	Hybrid nanofluid
s1	First nanoparticle (Cu)
s2	Second nanoparticle (Al_2O_3)
∞	Free stream condition
w	Wall condition

Conflicts of Interests: None

Source of support: None

REFERENCES

Arif, M., Saeed, A., Suttiarporn, P., Khan, W., Kumam, P., & Wathayu, W. (2022). Analysis of second grade hybrid nanofluid flow over a stretching flat plate in the presence of activation energy. *Scientific Reports, 12*, Article 21565.

Arrhenius, S. (1889). Über die Reaktionsgeschwindigkeit bei der Inversion von Rohrzucker durch Säuren. *Zeitschrift für Physikalische Chemie, 4*, 226–248.

Bejan, A. (1979). A study of entropy generation in fundamental convective heat transfer. *Transactions of the ASME, Journal of Heat Transfer, 101*, 718–725.

Bejan, A. (1996). *Entropy generation minimization*. CRC Press.

Boudebous, S., & Ferroudj, N. (2021). New approach to compute accurately the entropy generation due to natural convection in a square cavity. *E3S Web of Conferences, 321*, Article 04020.

Boudebous, S., & Ferroudj, N. (2023). Irreversibility distribution ratio used in entropy generation equation for convective flows re-visited. *E3S Web of Conferences, 321*.

Choi, S. U. S., & Eastman, J. A. (1995). Enhancing thermal conductivity of fluids with nanoparticles. In *ASME International Mechanical Engineering Congress & Exposition*, San Francisco, CA, USA.

Crane, L. J. (1970). Flow past a stretching plate. *Zeitschrift für Angewandte Mathematik und Physik, 21*(4), 645–647.

Dunn, J. E., & Rajagopal, K. R. (1995). Fluids of differential type: Critical review and thermodynamic analysis. *International Journal of Engineering Science, 33*(5), 689–729.

Maxwell, J. C. (1881). *A treatise on electricity and magnetism* (2nd ed.). Clarendon Press.

Pathak, T. S., Kim, J. H., Lee, S. J., & Baek, D. J. (2021). Preparation of aloe vera and sodium alginate-based hybrid nanofluid and its application in heat transfer. *Journal of Molecular Liquids, 335*, Article 116188.

Rajagopal, K. R. (1993). Mechanics of non-Newtonian fluids. In *Recent developments in theoretical fluid mechanics* (Vol. 291, pp. 129–162).

Rosseland, S. (1936). *Theoretical astrophysics: Atomic theory and the analysis of stellar atmospheres and envelopes*. Clarendon Press.

Sajid, M. U., & Ali, H. M. (2018). Thermal conductivity of hybrid nanofluids: A critical review. *International Journal of Heat and Mass Transfer, 126*, 211–234.

Sarkar, J., Ghosh, P., & Adil, A. (2015). A review on hybrid nanofluids: Recent research, development and applications. *Renewable and Sustainable Energy Reviews, 43*, 164–177.

Shukla, N., Rana, P., & Bég, O. A. (2019). Unsteady MHD non-Newtonian heat transfer nanofluids with entropy generation analysis. *Nonlinear Engineering, 8*(1), 630–644.

Solar radiation and energy of Arrhenius activation evaluation on a convectively heated stretching sheet flowing of Williamson hybrid nanofluid. (2024). *Indian Journal of Physics, 98*(5), 1745–1760.

Subbarao, K., Elangovan, K., & Gangadhar, K. (2022). Entropy analysis in a second-grade nanoliquid influenced by an exponential space-dependent heat source and Arrhenius activation energy. *Heat Transfer, 51*(6), 5679–5699.

Suresh, S., Venkitaraj, K. P., Selvakumar, P., & Chandrasekar, M. (2011). Synthesis of Al_2O_3-Cu/water hybrid nanofluids using two step method and its thermo physical properties. *Colloids and Surfaces A: Physicochemical and Engineering Aspects, 388*(1–3), 41–48.